energies

MDPI

Article

Determination of Pyrolysis and Kinetics Characteristics of Chicken Manure Using Thermogravimetric Analysis Coupled with Particle Swarm Optimization

Jie Gu [1], Cheng Tung Chong [1,*], Guo Ren Mong [2], Jo-Han Ng [3,4] and William Woei Fong Chong [5]

[1] China-UK Low Carbon College, Shanghai Jiao Tong University, Lingang, Shanghai 201306, China
[2] School of Energy and Chemical Engineering, Xiamen University Malaysia, Sepang 43900, Selangor, Malaysia
[3] Faculty of Engineering and Physical Sciences, University of Southampton Malaysia, Iskandar Puteri 79100, Johor, Malaysia
[4] Carbon Neutrality Research Group, University of Southampton Malaysia, Iskandar Puteri 79100, Johor, Malaysia
[5] Automotive Development Centre (ADC), Institute for Vehicle System & Engineering (IVeSE), Universiti Teknologi Malaysia, Skudai 81310, Johor, Malaysia
* Correspondence: ctchong@sjtu.edu.cn

Abstract: The valorization of chicken manure via pyrolysis can give biowaste a second life to generate value and contribute to the circular economy. In the present study, the thermal degradation and pyrolysis characteristics of chicken manure pyrolysis were investigated via thermogravimetric analyses (TGA) coupled with optimization methods. Thermogravimetric data were obtained for the samples at five heating rates of 5, 10, 20, 30 and 50 °C/min over a range of temperature under inert conditions. The manure devolatilization process was initiated at between 328 and 367 °C to overcome the global activation energy barrier. The determined activation energy of the manure via Flynn–Wall–Ozawa (FWO), Kissinger–Akahira–Sunose (KAS), Friedman and Kissinger methods was in the range of 167.5–213.9 kJ/mol. By using the particle swarm optimization (PSO) method, the pyrolytic kinetic parameters of the individual component present in the manure were calculated, in which the activation energy for cellulose (227.8 kJ/mol) was found to be higher than that of hemicellulose (119 kJ/mol) and lignin (134.3 kJ/mol). Based on intrinsic transition-state theory, the pre-exponential factor and activation energy of the manure can be correlated through a linear equation $\ln A_\alpha = 0.2006\, E_\alpha - 1.2847$. The devolatilization characteristics of the chicken manure were elucidated via the optimization process, paving the way for the design of thermochemical conversion reactors and processes.

Keywords: pyrolysis; chicken manure; thermogravimetric analysis; kinetic analysis; particle swarm optimization

Citation: Gu, J.; Chong, C.T.; Mong, G.R.; Ng, J.-H.; Chong, W.W.F. Determination of Pyrolysis and Kinetics Characteristics of Chicken Manure Using Thermogravimetric Analysis Coupled with Particle Swarm Optimization. *Energies* **2023**, *16*, 1919. https://doi.org/10.3390/en16041919

Academic Editors: Chew-Tin Lee, Yee-Van Fan, Jiří Jaromír Klemeš and Norhuda Binti Abdul Manaf

Received: 17 December 2022
Revised: 23 January 2023
Accepted: 31 January 2023
Published: 15 February 2023

1. Introduction

Most nations in the world have bound together to tackle global climate change through the legally binding international treaty the Paris Agreement, with the aim of reducing emissions of greenhouse gas. One of the most pertinent goals of the agreement is to keep the global temperature rise to 2 °C, if possible to within 1.5 °C, by the mid 21st century [1]. Hence, most countries have pledged to achieve carbon neutrality goal by 2050 or 2060, that is to decarbonise various sectors to attain net-zero carbon emissions [2]. To reduce dependence on fossil fuels, much effort has been dedicated to developing sustainable and environment-friendly fuels using biomass or agro-industrial wastes [3,4]. Among the bioresources, manure from farmed poultry present a valuable feedstock for valorization to obtain bioenergy and valuable derivatives [5], which can contribute to the circular economy while reducing carbon footprint.

The global consumption of poultry meat is in an increasing trend owing to the rapid development of the economy and the improvement of living standards. At present, over 80% of global meat demand is met by poultry, amounting to more than 130 million metric tonnes of poultry meat production on average [6]. Among farmed poultry, chicken tops the global consumption list due to its affordable price and protein-rich content, with China, the U.S., Indonesia, India and Mexico being the top chicken meat producing countries [7]. Large-scale chicken farming to meet the demands of a large population inevitably leads to the production of biological waste of chicken manure, which requires proper disposal and management to avoid environmental pollution. Traditional methods of composting are among the commonly used methods of converting manure into soil fertilizer to make use of the mineral-rich content [8]. Even though the composted manure can be used as a soil ameliorant, the presence of harmful pathogens and toxic gases such as ammonia risks harming the environment and human beings [9]. In addition, the presence of heavy metal trace elements such as As, Pb or Cu in chicken manure present leaching risks, resulting in problems such as eutrophication and soil contamination [10].

Anaerobic digestion (AD) is a biochemical conversion method that can be deployed to convert livestock manure into biogas (a mixture of CH_4 and CO_2) for energy recovery [11], but the limitations of the techniques include the need to accurately regulate the bioreactor conditions, deactivation of microbial activities and generation of toxic gases from the anerobic activities [12]. The use of the thermochemical conversion process is another effective way to dispose of poultry manure [13] while recuperating bioenergy through the oxidation process [14]. The direct burning of manure is the most direct way to recover energy, and has the advantage of eliminating germs or pathogens at high temperature, but the release of unburned hydrocarbons (UHCs), particulate matters (PMs), volatile organic compounds(VOCs) and polycyclic aromatic hydrocarbons (PAHs) generated during the combustion process are hazardous to the environment and human health [15]. Pyrolysis is another thermal process that can valorize manure into non-condensable gases comprising CO, CO_2, H_2 and CH_4, alongside liquid bio-oil and solid biochar [16]. The synthesis gas produced can be used as platform gas to synthesize high-value ammonia, methanol and other industrial products [17]. Bio-oil is recognized as an important alternative fuel [18], while the biochar produced can be used for soil improvement or as solid fuel [19]. Apart from recovering useful byproducts [20], the highly efficient pyrolysis process can effectively eliminate pathogens and inhibit the formation of harmful gas, as the reactor is operating at 400 to 700 °C. Further, the emissions of air pollutants such as NO_x, SO_x, dust particles and dioxins can be significantly reduced compared with direct combustion [21].

The thermochemical conversion of animal waste into different by-products undergoes a series of complex thermal decomposition processes, during which various chemical reactions take place. Kinetic analysis is an effective method to predict the kinetics and reaction behavior during the thermal degradation of the feedstock. Such studies are often conducted via thermogravimetric analysis [22]. Dhyani et al. [23], have computationally demonstrated that the Flynn–Wall–Ozawa (FWO) and Kissinger–Akahira–Sunose (KAS) methods are capable of predicting the reaction kinetic parameters at high conversion rates. Many scholars have used various model-free kinetic modeling methods when studying solid-state kinetic TGA under non-isothermal processes [24–26]. Cao et al. [27] studied the pyrolysis behavior of cow dung and determined the activation energy of the manure is in the range of 125–444 kJ/mol via the distributed activation energy model (DAEM). Such value differs from those of horse manure, which was about 200 kJ/mol determined via the Flynn–Wall–Ozawa (FWO), Kissinger–Akahira–Sunose (KAS) and Friedman methods [28], reflecting the varied pyrolysis characteristics of different manures. Fernandez-Lopez et al. [29] utilized the DAEM and pseudo-multi-component stage model (PMSM) to predict swine manure pyrolysis weight loss curves, and concluded that the former fitted well with the experimental data.

Despite some previous studies on the thermochemical processes of livestock manure, there is a lack of optimized kinetics data for poultry manure, which is needed for pyrolysis

modelling. In the present study, the pyrolysis characteristics of farmed chicken manure are determined using thermogravimetric analyses at different heating rates, followed by determination of the kinetic and thermodynamic properties using different model-free fitting methods. By coupling this method with the particle swarm optimization (PSO) model, the pyrolytic kinetic parameters of the complex composition of manure are further resolved to component level. The PSO is a population-based stochastic optimization technique based on the principles of the swarming behavior of a group of organisms, i.e., insects, herds, birds or fish, in search of food in a cooperative manner. The algorithm optimizes the calculation of the internal velocity and position of each particle by iterating its own experience and those of members nearby under search mode [30]. The optimized parameters obtained from the PSO model are used for curve fitting and compared to the experimental data. Apart from understanding the pyrolytic behavior of chicken manure, the predicted thermodynamic and kinetic data obtained from the optimization model can serve as a guide for thermochemical conversion process design.

2. Experimental Section

2.1. Feedstock Preparation and Characterization

The chicken manure used in the experiment was collected from a poultry farm located at Rudong County, Nantong, Jiangsu province, China. The fresh manure was first air-dried by natural air, followed by electric drying in an oven at 110 °C for 12 h to remove the moisture [31]. The dried manure was then ground and sieved through a No. 40 size mesh sieve to obtain the powdered form. Analysis of the manure's elemental composition was conducted via an elemental analyzer (Elementar, Vario EL Cube) to determine the basic CHNS compounds, while the O element was determined by an organic element analyzer (ThermoFisher, Flash Smart). For the purpose of quantifying the moisture content, volatile matter and ash content, proximate analysis was conducted via a thermogravimetric analyzer (PerkinElmer, TGA 8000). The trace elements in the manure were characterized via a plasma emission spectrometer (Thermo Elemental, iCAP6300).

2.2. Thermogravimetric Analysis

The pyrolysis behavior of chicken manure was examined through a thermogravimetric analysis at the heating rate of 5, 10, 20, 30 and 50 °C/min under inert N_2 conditions [32]. Prior to the experiment, the thermogravimetric analyzer was flushed with N_2 at a flow rate of 100 mL/min to prevent sample oxidation, followed by heating the 12 mg sample placed in the crucible from room temperature to 700 °C at a fixed heating rate. The remaining residue left after the pyrolysis was assumed to be char and ash.

2.3. Analysis of the Kinetic Parameters

Thermogravimetric analysis was used to explore the kinetic parameters of solid thermal decomposition. Coupled with the model-free methods, the main kinetic parameters during the pyrolysis process such as activation energy (E_α) and pre-exponential factor (A) could be determined. The specific reaction model of pyrolysis was established by the relationship between the conversion rate and conversion range [23]. The conversion rate of the manure sample was defined as the mass fraction of decomposed solids, as shown in the following equation:

$$\alpha = \frac{m_0 - m}{m_0 - m_\infty} \tag{1}$$

where m_0, m and m_∞ are the initial, instantaneous and final masses of the solid, respectively. The rate of conversion of feedstock α, which is dependent on temperature is expressed as:

$$\frac{d\alpha}{dt} = k(T)f(\alpha) \tag{2}$$

where t represents time, $k(T)$ is reaction, which is a temperature-dependent (in kelvin) term, and $f(\alpha)$ is the reaction model. Temperature dependency of the reaction rate constant can be shown by the Arrhenius equation as follows:

$$k(T) = Aexp\left[-\frac{E_\alpha}{RT}\right] \tag{3}$$

where A is the pre-exponential factor or frequency factor (min^{-1}), E_α is activation energy (J/mol), T denotes the absolute temperature and R is the universal gas constant (J/mol·K).

In non-isothermal degradation, combining Equations (2) and (3) yields:

$$\frac{d\alpha}{dt} = kf(\alpha) = Aexp\left[-\frac{E_\alpha}{RT}\right]f(\alpha) \tag{4}$$

The temperature is related to time, t, through the equation:

$$T_t = T_0 + \beta \times t \tag{5}$$

where T_0 is the initial temperature and β is the heating rate. By relating time t and temperature T, the expression of the conversion rate in Equation (4) can be established with respect to temperature T under non-isothermal condition via:

$$\frac{d\alpha}{dT} = \frac{A}{\beta}\exp\left[-\frac{E_\alpha}{RT}\right]f(\alpha) \tag{6}$$

by integrating Equation (6), we can get the following:

$$\int_0^\alpha \frac{d\alpha}{f(\alpha)} = \int_0^T \frac{A}{\beta}exp\left(-\frac{E_\alpha}{RT}\right) \times dT \tag{7}$$

Since $\int_0^{T_0} \frac{A}{\beta}exp\left(\frac{-E_\alpha}{RT}\right) \times dT = 0$, the equation reduces to:

$$g(\alpha) = \int_{T_0}^T \frac{A}{\beta}exp\left(\frac{-E_\alpha}{RT}\right) \times dT \tag{8}$$

Since in this experiment, the reaction rate and conversion rate are determined by temperature, and the reaction mechanism and kinetics do not need to be assumed in the calculation process, three iso-conversional model-free methods are chosen to determine the E_α and A from the TGA data, namely the Flynn–Wall–Ozawa (FWO), Kissinger–Akahira–Sunose (KAS) and Friedman methods. Another model-free method of Kissinger is adopted to evaluate the E_α value from the entire reaction.

2.3.1. Flynn–Wall–Ozawa Method (FWO)

Bianchi et al. [33] effectively determined the kinetic parameters of the reaction by using TG and DSC (differential scanning calorimetry) curves on the basis of the FWO method. The method is based on the Doyle approximation for heterogeneous chemical reactions:

$$\ln(\beta_i) = \ln\left(\frac{A_\alpha R}{E_\alpha f(\alpha)}\right) - 5.331 - 1.052\frac{E_\alpha}{RT_{\alpha i}} \tag{9}$$

When applying the FWO method, the basic assumption is that the reaction rate at a given conversion is only temperature dependent. Therefore, by plotting five sets of points of heating rate ln β as a function of $1/T$ at the same conversion rate and fitting into a straight line, the slope of the straight line $-1.052\ E_\alpha/R$ is the required activation energy.

2.3.2. Kissinger–Akahira–Sunose Method (KAS)

The Kissinger–Akahira–Sunose (KAS) method uses the Coats–Redfern approximation to correct some of the biases present in the FWO method [34]. Therefore, the Arrhenius equation for KAS is expressed as:

$$ln\left(\frac{\beta_i}{T_{\alpha i}^2}\right) = ln\left(\frac{A_\alpha R}{E_\alpha f(\alpha)}\right) - \frac{E_\alpha}{RT_{\alpha i}} \quad (10)$$

The activation energy is calculated from the slope $(-E_\alpha/R)$ of the linear equation between ln β/T^2 and $1/T$.

2.3.3. Friedman Method

The Friedman method has been commonly used to evaluate the activation energy of a reaction in a differential iso-conversional method. It establishes a functional relationship between the reciprocal of temperature and the conversion rate under a logarithmic function, [35], which is expressed as:

$$ln\left(\frac{d\alpha}{dt}\right)_{\alpha_i} = ln[A_\alpha \times f(\alpha)] - \frac{E_\alpha}{RT_{\alpha_i}} \quad (11)$$

By plotting five pairs of ln $(d\alpha/dt)$ and $1/T$ data points from all five heating rates at the same conversional fraction, the slope $-E_\alpha/R$ of the fitting straight line can be used to calculate the activation energy.

2.3.4. Kissinger Method

The Kissinger method is widely used in the literature to calculate the activation energy of the reaction, based on the following expression:

$$ln\left(\frac{\beta}{T_p^2}\right) = ln\left(\frac{AR}{E}\right) - \frac{E}{RT_p} \quad (12)$$

Kissinger's method is one of the most commonly used non-isothermal methods to determine kinetic parameters through thermal analysis. The Kissinger peak displacement method can be adopted in conjunction with differential scanning calorimetry, is suitable for small sample sizes and allows efficient determination of the dynamic parameters [36]. When determining the activation energy E, the peak temperature T_P that occurs during thermal decomposition is used to plot the graph of ln $(\beta/{T_p}^2)$ vs. $1/T_p$. Activation energy is calculated from the gradient of the straight-line graph which is equal to $-E_\alpha/R$.

2.3.5. Kinetic Reactions Scheme

Since chicken manure is mainly composed of lignocellulosic biomass [37], the reaction mechanism of pyrolysis for the main component can be expressed as:

$$Component \Rightarrow \lambda_i Volatiles_i + \delta_i Char_i \quad (13)$$

The reaction mechanism showed that the components were converted into volatiles and char after the reaction, where λ_i and δ_i are the mass fractions of volatiles and char for each component i ($\lambda = 1 - \delta$). Based on the nth order reaction-order model, the reaction rate of each component can be expressed as:

$$\frac{dW_i}{dt} = -A_i exp(-\frac{E_i}{RT})W_{i,0}(\frac{W_i}{W_{i,0}})^{n_i} \quad (14)$$

$$\frac{d\alpha_i}{dt} = -A_i exp(-\frac{E_i}{RT})(1-\alpha_i)^{n_i} \quad (15)$$

In the formula, W_i represents the instantaneous mass, A_i and E_i are the pre-exponential factor and activation energy, respectively, n_i is the reaction order, and the subscript i represents each corresponding component. For each component i, W_i represents the mass fraction of this component, and $W_{i,0}$ represents the initial mass fraction of this component in the raw material. When pyrolysis is complete, the rate of production of char, W_{char}, is assumed to be constant:

$$\frac{dW_{char,i}}{dt} = \sum_{i=1}^{n} \delta_i W_{i,0} \frac{d\alpha_i}{dt} \tag{16}$$

Therefore, the mass loss rate curves can be expressed as:

$$\left(\frac{dW}{dt}\right)_{cal} = \sum_{i=1}^{n} \frac{dW_i}{dt} + \frac{dW_{char,i}}{dt} \tag{17}$$

The final solid content includes unreacted components in the feedstock as well as the resulting char, the mass of which can be expressed by the following:

$$W_{cal}(t) = 1 - \sum_{i=1}^{n} \lambda_i \alpha_i W_{i,0} \tag{18}$$

The established kinetic model is subsequently used to predict the thermodynamic parameters of the pyrolysis process.

2.4. Global Optimization Technique—Particle Swarm Optimization

Particle swarm optimization (PSO) is a population-based stochastic optimization technique based on the principles of the swarming behavior of a group of organisms, i.e., insects, herds, birds or fish, in search of food in a cooperative manner. The algorithm optimizes the calculation of the internal velocity and position of each particle by iterating its own experience and those of members nearby under search mode [30]. The PSO method is selected over other standard heuristic algorithms such as the bacterial aging optimization algorithm (BFOA) and artificial bee colony (ABC), as it does not require prerequisites such as continuity or differentiability of the objective function [38]. In addition, when compared with the genetic algorithm (GA) [38] and shuffled complex evolution (SCE) [39] algorithms (often used as an optimization for local and global problems), the PSO method also has the advantages of good optimization ability, while providing faster approximation to the global optimal solution [40].

Assuming that all n particles are free to search for the best position in the n-dimensional space, the position of the ith particle in the n-dimensional space is denoted as x_i, and the velocity is denoted as v_i. For the present work's objective function, each particle will obtain a fitness value according to the requirements, and on the basis of knowing its current position x_i, it continuously receives information on the individual optimal value and the global optimal value (p_i and p_g, respectively). Thereby, the next location update is performed. The position update of each particle is represented by the following formula:

$$V_{ij}^{k+1} = \varepsilon V_{ij}^{k} + c_1 r_1 \left(p_{ij} - x_{ij}^{k}\right) + c_2 r_2 \left(P_{gj} - x_{ij}^{k}\right) \tag{19}$$

$$x_{ij}^{k+1} = x_{ij}^{k} + v_{ij}^{k+1} \tag{20}$$

where i, j represent the particle and its search direction (from 1 to J), ε is the inertia weight, k is the number of iterations, p_{ij} is the best individual particle position, and p_{gj} is the global best position for all the particles. The two acceleration constants representing individual particles and the global population in the selected particle population are denoted by c_1 and c_2, r_1 and r_2, randomly selected between [0, 1], are the coefficients. For the pyrolysis experiments in this paper, the parameters to be optimized include activation energy (E_i), pre-exponential factor (A_i), reaction order (n_i), initial mass fraction of each component

($W_{i,0}$) and carbon yield (δ_i). The following objective function φ is defined as the error of mass loss and mass loss rate under experimental conditions and the kinetic model, where the calculated mass loss and mass loss rate are given in Equations (17) and (18):

$$\varphi = \omega \sum_{1}^{k} \frac{\sum_{1}^{n_d} \left(W_{cal,i} - W_{exp,i}\right)^2}{\sum_{1}^{n_d} W_{exp}^2} + (1-\omega) \sum_{1}^{k} \frac{\sum_{1}^{n_d} \left(\left(\frac{dw}{dt}\right)_{cal,i} - \left(\frac{dw}{dt}\right)_{exp,i}\right)^2}{\sum_{1}^{n_d} \left(\frac{dw}{dt}\right)_{exp}^2} \quad (21)$$

In the objective function φ, the subscript *exp* represents the numerical values obtained by the experiment, and *cal* represents the numerical values obtained by the calculation. W represents the value of mass loss in the pyrolysis process, (dw/dt) is the mass loss rate, k represents the different heating rates selected in the TGA experiment, and n_d is the data point selected under each group of heating rates. ω is the weight coefficient occupied by the two parts of the formula (mass loss and mass loss rate), and ω = 0.5 is taken because the weight loss value and the weight loss rate are guaranteed to have equal proportions during the calculation. For this study, to achieve the best optimization effect, the basic parameters applicable to particle swarm optimization: swarm size, dimension of optimization, maximum speed, inertia parameter and maximum number of iterations were determined to be 60, 14, 0.1, 0.9, and 2000, respectively. The PSO algorithm calculation steps were realized in MATLAB@ (version R2012a) software, using an Intel(R) Core(TM) i7-10750H CPU @ 2.60 GHz 2.59 GHz. Figure 1 illustrates the process flow of the PSO algorithm.

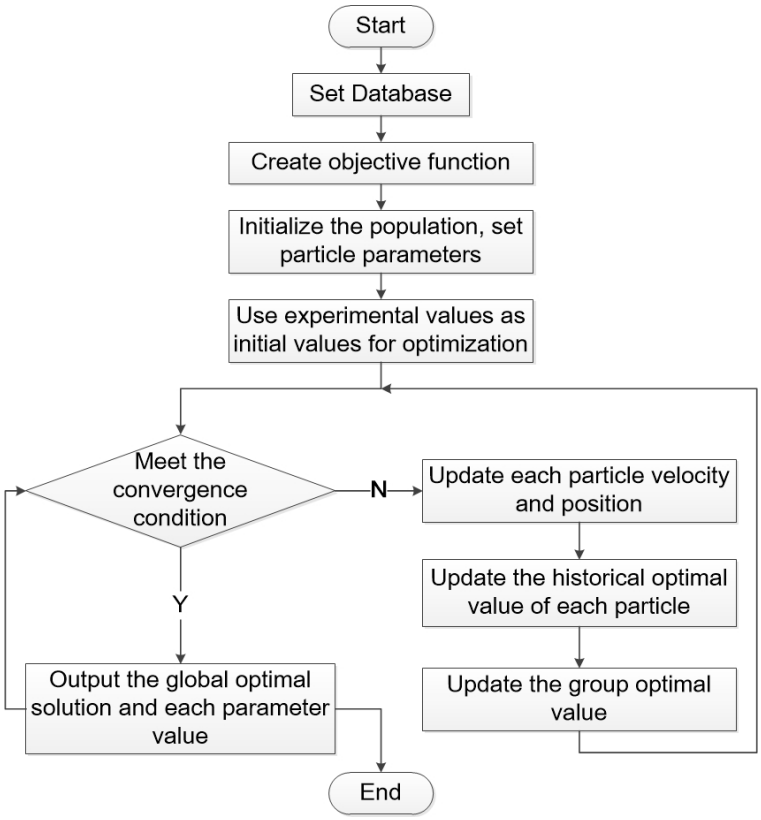

Figure 1. Process flowchart of the PSO algorithm.

The quality of fitting between the predicted and experimental thermal degradation curves is evaluated via Equation (22) [41]:

$$Fit(\%) = \left(1 - \frac{\sqrt{\frac{S}{N}}}{\left(P_{exp}\right)_{max}}\right) \times 100\% \quad (22)$$

When calculating the quality of fitting for TG curves, $S = \sum_1^{n_d} \left(W_{cal,i} - W_{exp,i}\right)^2$ and P_{exp} represents the experimental weight, whereas the quality of fitting for DTG curves is determined via $S = \sum_1^{n_d} (\left(\frac{dw}{dt}\right)_{cal,i} - \left(\frac{dw}{dt}\right)_{exp,i})^2$ and P_{exp} represents the experimental $\frac{dw}{dt}$. N is the number of experimental points under both cases. The calculated result shows the fit quality between the optimization results and the experimental data.

2.5. Thermodynamic Parameters

Each type of biomass has its own distinct pyrolysis characteristics. Deriving the thermodynamic parameters of the raw materials elucidates the pyrolytic and decomposition characteristics under specific conditions. The thermodynamic parameters involved in this paper mainly include the pre-exponential factor (A), changes of enthalpy (ΔH), free Gibbs energy (ΔG) and entropy (ΔS), as shown in the equations listed in Table 1.

Table 1. Thermodynamic parameters equation [42].

Thermodynamic Parameters	Equation
Pre-exponential factor, A	$A = \beta E_\alpha exp\left(\frac{E_\alpha}{RT_p}\right) / \left(RT_p^2\right)$
Changes of enthalpy, ΔH	$\Delta H = E_\alpha - RT$
Free Gibbs energy, ΔG	$\Delta G = E_\alpha + RT_p ln\left(\frac{K_B T_p}{hA}\right)$
Entropy, ΔS	$\Delta S = \frac{\Delta H - \Delta G}{T_p}$

K_B is the Boltzman constant (1.281×10^{-23} J/K), h is the Plank constant (6.626×10^{-34} Js), T_p is the DTG peak temperature, and T_α is the temperature at the conversion degree, α.

3. Results and Discussion

3.1. Sample Characterization

The ultimate analysis shows that chicken manure has high content of C and O relative to the H element, while the presence of N and S are in trace amounts (<1% wt), as shown in Table 2. From the results of the proximate analysis, the ash content in chicken manure is higher than crop straws (10 wt%) [41], due to the fact that chicken manure contains more straw-like substance, which is prone to produce ash. The high content of carbon in the manure indicates its potential for thermochemical conversion [43]. Analysis of the trace elements, shown in Table 3, indicates that K, Ca, Na, Mg and O are the dominant minerals present in the chicken manure, owing to the excessive nutrients from the feeds that are not being fully absorbed by the short digestive system of chickens. The presence of other elements such as Cu and Zn is attributed to the use of antibiotics [44]. Other alkali metals that were present, such as Na and K, are known to have reactive catalytic properties during thermoconversion process [45].

Table 2. Ultimate and proximate analysis of chicken manure.

Ultimate Analysis (wt%)	
Carbon	31.2
Hydrogen	5.0
Nitrogen	0.9
Oxygen	34.4
Sulphur	0.7
Proximate Analysis (wt%)	
Moisture	4.1
Volatile	48.1
Fixed Carbon [a]	19.1
Ash	28.8

[a] calculated by difference.

Table 3. Trace element analysis of chicken manure.

Trace Elements	mg/kg
K	24,164.2
Ca	21,097.9
Mg	6268.1
Na	5944.5
P	3286.5
Al	991.0
Fe	586.0
Zn	240.9
Si	48.1
Cu	41.3

3.2. Thermogravimetric Analysis (TGA)

The pyrolysis characteristics of chicken manure were examined using thermogravimetric analysis at five different heating rates of 5, 10, 20, 30 and 50 °C/min, as shown in Figure 2a. The degradation of chicken manure shows distinct weight loss in the temperature ranges of 30–150 °C (Stage I), 150–500 °C (Stage II) and ≥500 °C (Stage III), which corresponds to the dehydration, primary and secondary devolatilization stages. The dehydration range removes moisture from the manure, while the latter two involve the decomposition of hemicellulose, cellulose and lignin in the different temperature ranges. Such a process is similar to the pyrolysis behavior of cattle manure [31], most probably due to the consumption of a plant-based diet. The pyrolysis peak temperature of chicken manure is between that of cow manure and ordinary lignocellulosic biomass, owing to the extracts such as protein, starch and lipids in manure that result in a drop in pyrolysis peak temperature. The decomposition of the extract is a non-negligible part of the pyrolysis process [46].

It can be clearly seen in the DTG curve shown in Figure 2b that the first peak of chicken manure pyrolysis appears around 140 °C and the second peak appears between 300–400 °C. This corresponds to the evaporation of moisture and the breakdown of hemicellulose and cellulose, respectively. Within the temperature range of 300–400 °C, there are two peaks at 300 °C and 350 °C, which are related to the thermal degradation of the hemicellulose and cellulose, respectively [47]. When comparing the DTG curves, it can be seen that, as the heating rate increases from 5 to 50 °C/min, the overall weight loss curve gradually shifts to the right. This is because a lower heating rate allows more time for heating to occur, leading to a better heat transfer effect to achieve thermal equilibrium. The lower heating rate also results in the onset of peak pyrolysis temperature. The conversion rate corresponding to the three regions of pyrolysis is shown in Figure 2c. The results show that about 12.5% of the feedstock was thermally decomposed at 200 °C, while the main bulk of mass was devolatilized at 400 °C, accounting for about 80% conversion. The remaining lignin component was converted at above 500 °C.

Figure 3 shows the second derivative curve of m_t/m_0 (DDTG) for the second stage of pyrolysis. Taking the heating rate of 30 °C/min as a representative case, the process before 100 °C is ascertained as the evaporation of moisture; hence the initial starting point of the DDTG curve is taken as 100 °C. With zero gradient as the reference line, the second stage of the thermal devolatilization of chicken manure can be further divided into three subsections, i.e., section I (176.5–320.4 °C), section II (320.4–416.8 °C) and section III (416.8–497.7 °C), which corresponds to the degradation of hemicellulose, cellulose and lignin. Within the range of 100–325 °C, hemicellulose is decomposed. A strong peak can be seen in between 325 °C and 410 °C, where a significant portion of cellulose is degraded before stabilizing in the third region, where lignin degradation continues to occur [48].

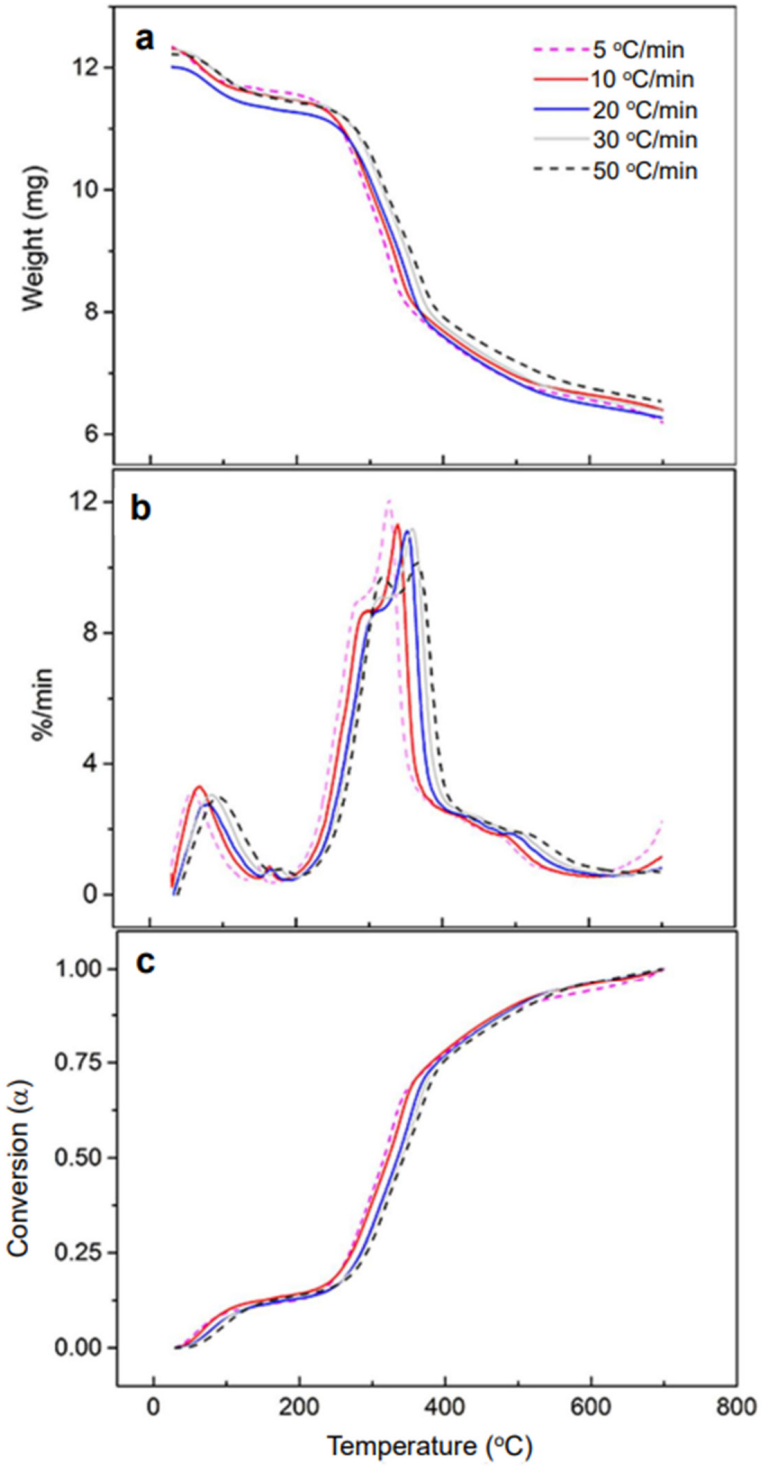

Figure 2. (**a**) TG, (**b**) DTG and (**c**) conversion curve derived from the thermogravimetric analysis of chicken manure.

3.3. Kinetic Analysis

Kinetic analysis of the chicken manure was performed within the pyrolysis region minus the influence of moisture to ensure the fidelity of the data [49]. In the present study, the kinetic calculations were performed using at the conversion fraction range of 0.2–0.7 at the interval of 0.1.

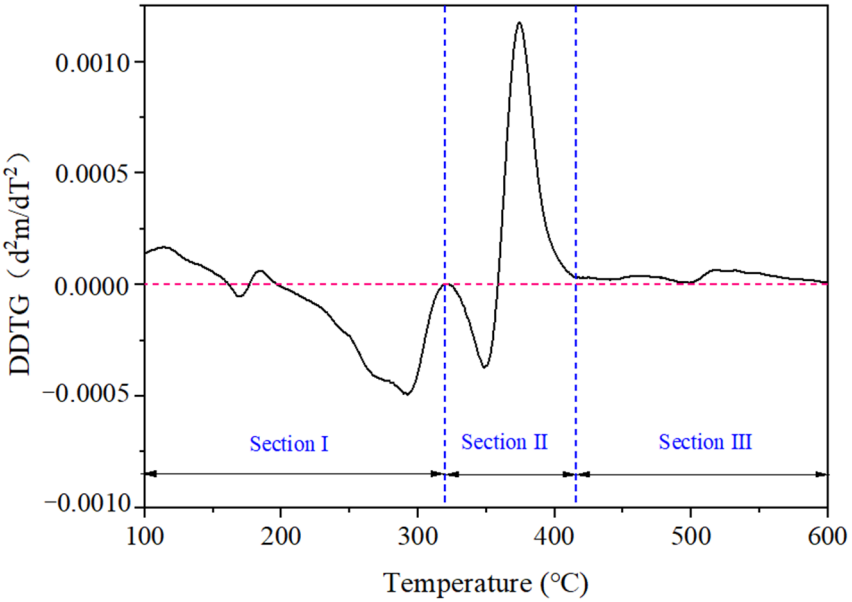

Figure 3. DDTG curve of Stage II using second derivative method. Section I, II and III correspond to the degradation of hemicellulose, cellulose and lignin.

3.3.1. Activation Energy

In the present work, the activation energy and pre-exponential factor of chicken manure were calculated by four model-free methods, FWO, KAS, Friedman and Kissinger. On the basis of these four models, we used Equations (9)–(11) to plot the linear regression curves at all the selected conversion rates. Figure 4 shows the conversional fraction for chicken manure obtained at various heating rates using the FWO, KAS and Friedman methods. These methods were observed to exhibit a linear trend for most conversion fraction except at α = 0.2 and 0.7, owing to the instability at the beginning and near the end of the reaction. Table 4 summarizes the value of E_α derived from the slopes for each method. The activation energy values for each conversional rate, along with the correlation coefficient R^2, were tabled to reflect the level of thermal decomposition of feedstock at different stages. A variation of activation energy at different conversion rates was expected, owing to the variety in component degradation. Activation energy was generally higher in the mid-section of $\alpha > 0.4$, due to the higher energy barrier imposed by cellulose and lignin; thus the local activation energy ranged between 195.5 and 249.4 kJ/mol, 192.8 and 208.5 kJ/mol and 203.4 and 362.4 kJ/mol, for the FWO, KAS and Friedman methods, respectively. The Friedman method showed overall higher local activation values than the FWO and KSA methods. The average activation energy for the chicken manure was determined to be 206.13 kJ/mol (FWO), 200.55 kJ/mol (KAS) and 231.93 kJ/mol (Friedman), while the R^2 correlations of >0.95 show the reliability of the linear regression.

When the Kissinger method is used to calculate activation energy, it mainly depends on the peak temperature in the thermogravimetric curve. In addition to the weight loss peak of water in the raw material that can be clearly identified, the decomposition of other components is within a certain range, which can be seen from the thermogravimetric curve where a major weight loss peak occurs within this range. The peak temperature of this peak at different heating rates are selected as T_p (634, 653, 669, 688 and 690 K for heating rates of 5 °C, 10 °C, 20 °C, 30 °C and 50 °C, respectively). Figure 5 shows the linear fit line with a good correlation coefficient of $R^2 > 0.99$. The overall E_α and A obtained from the Kissinger method were 167.51 kJ/mol and 9.52×10^{13} s^{-1}, respectively. The calculated kinetics and thermodynamics parameters values are shown in the parameters in Table 5. Figure 6 shows the results of the activation energies obtained by each method at all the selected conversion rates. The FWO and KAS show almost identical trends, peaking at α = 0.7. The Friedman method shows a consistently higher local activation value across all conversion fractions,

with a trend of increase E_α with conversion fraction, peaking at $\alpha = 0.4$ before decreasing again. This is in contrast with the lower values derived using the FWO and KAS methods, which are based on the heating rate. The final part of $\alpha > 0.65$ requires higher activation energy to decompose the lignin, as reflected in all the methods. Further, the sudden increase in activation energy may also be due to changes in the pyrolysis mechanism and in situ catalysis of metals contained in the ash [50].

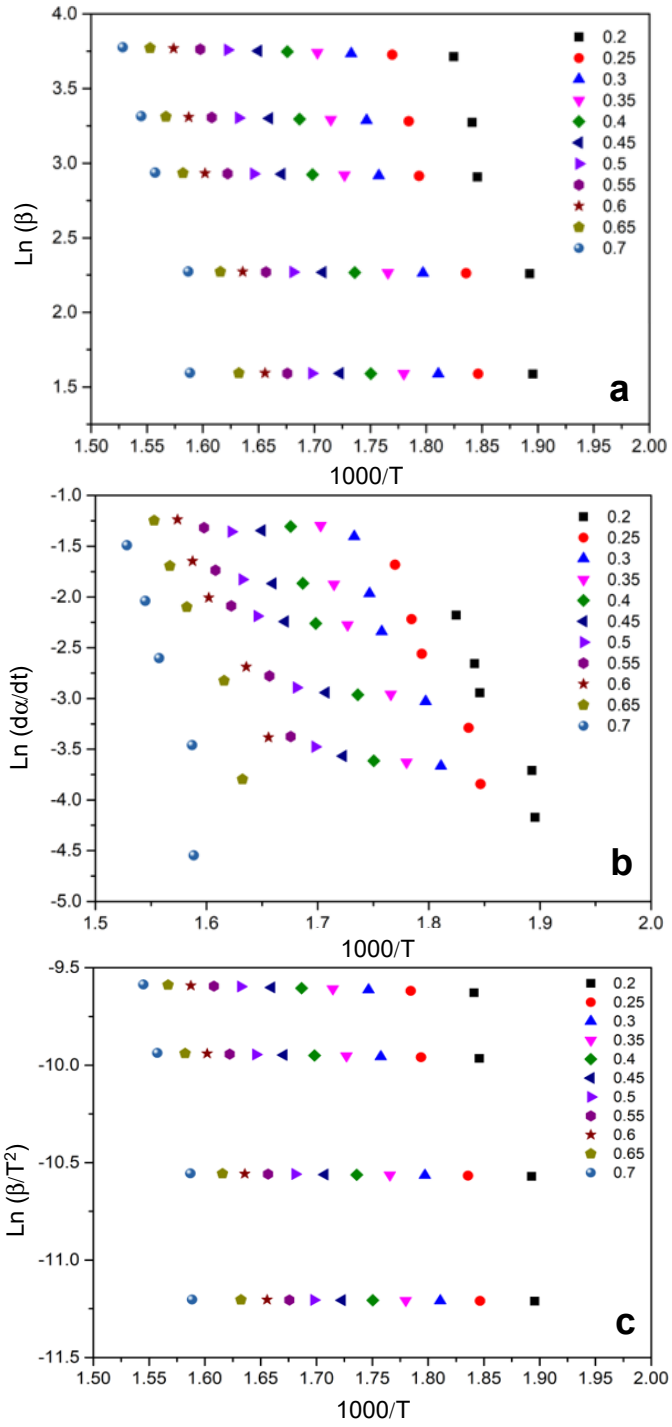

Figure 4. The conversional fractions for (**a**) FWO, (**b**) KAS and (**c**) Friedman methods for chicken manure derived at various heating rates.

Table 4. The activation energy for chicken manure derived from FWO, KAS and Friedman methods.

Method Conversion	FWO		KAS		Friedman	
	E_α (kJ/mol)	R^2	E_α (kJ/mol)	R^2	E_α (kJ/mol)	R^2
0.2	197.89	0.89	194.99	0.89	203.40	0.94
0.25	195.48	0.95	192.76	0.94	209.99	0.96
0.3	197.18	0.96	195.89	0.96	217.04	0.96
0.35	198.56	0.96	202.86	0.96	223.72	0.96
0.4	205.58	0.96	208.52	0.96	230.12	0.96
0.45	211.28	0.96	204.61	0.96	228.45	0.96
0.5	207.28	0.97	194.50	0.97	215.62	0.98
0.55	203.47	0.98	195.89	0.98	205.79	0.99
0.6	198.31	0.99	202.86	0.98	207.44	0.99
0.65	203.03	0.98	208.52	0.98	247.24	0.96
0.7	249.35	0.91	204.61	0.90	362.39	0.88
Mean	206.13	0.96	200.55	0.95	231.93	0.96

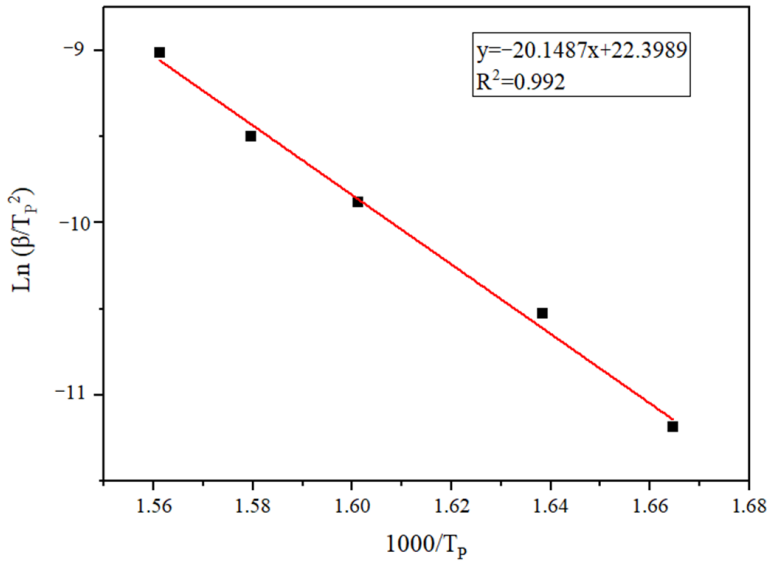

Figure 5. Kinetic parameter fitting curve under Kissinger method.

Table 5. Kinetics and thermodynamics parameters value calculated by Kissinger method. (Derived based on the T_p from five different heating rates).

Kissinger				
A (s^{-1})	E_α (kJ/mol)	ΔH (kJ/mol)	ΔG (kJ/mol)	ΔS (J/mol)
9.52×10^{13}	167.51	162.52	157.01	91.77

The Kissinger method showed a consistently lower activation energy than the other methods. The method assumes the reaction has reached a maximum reaction rate at peak temperature, independent of the reaction order. A possible reason for the lower E_α value could be due to the reaction order that is not equal to unity [51]. The FWO and KAS methods were shown to provide more accurate kinetic analysis and to be less affected by experimental error [52].

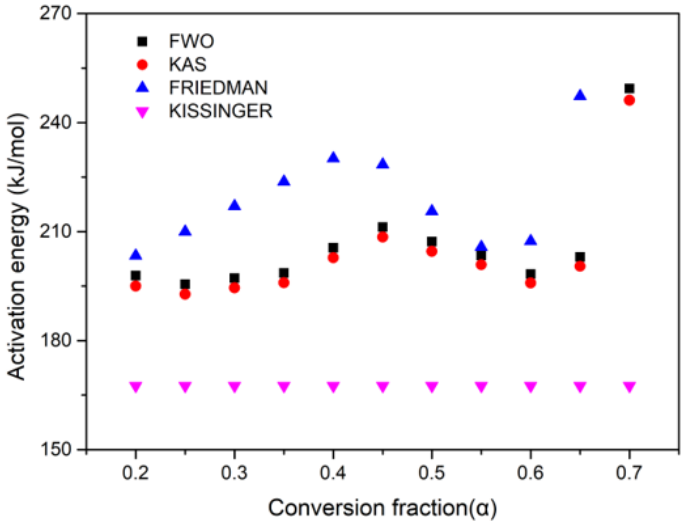

Figure 6. Activation energy of chicken manure obtained through FWO, KAS and Kissinger methods at different conversion rates.

3.3.2. Reaction Model and Pre-Exponential Factor

The E_α obtained by KAS and FWO methods were utilized to predict the pyrolytic parameters of chicken manure and to determine the relevant response model and pre-exponential factors. From the TGA and DDTG curves, the different peaks clearly show a complex process, which means the pyrolysis of chicken manure is not a single-step reaction. A simple single-step reaction mechanism is insufficient to describe the complete pyrolysis process of chicken manure. Solid-state pyrolysis reactions such as those that take place in chicken manure often occur between lattices or molecules that must penetrate the lattice. Under these conditions, the reaction is not controlled by mass transfer, and the diffusion effect becomes the main factor affecting the reaction rate [53]. Therefore, a more accurate model is needed to account for these effects. Due to the multi-component nature of chicken manure, different pyrolysis mechanisms should be used for different conversion rates during the pyrolysis process. To further explore the biomass pyrolysis model and mechanism, Xu et al. [54] plotted the experimental (scatters) and theoretical (lines) master plots as a function of conversion α. It was concluded that the pyrolysis process of such biomass resembled the model D3, while the associated mechanism was three-dimensional diffusion (Jander equation). Hence, the three-dimensional diffusion (Jander equation) proposed by Khawam et al. [53] was utilized for the analysis of the pyrolysis mechanism.

The ln A_α can be calculated via the E_α and the three-dimensional diffusion (Jander equation) $f(\alpha) = (3/2)\ [(1-\alpha)^{2/3}]/[1-(1-\alpha)^{1/3}]$ using Equation (11), based on the relationship that connects E_α and A_α, which is referred to as a compensation effect:

$$\ln A_\alpha = aE_\alpha + b \tag{23}$$

where a and b are the compensation effect numbers, which are constants. For the pyrolysis of chicken manure, this compensation effect is mainly caused by systemic errors produced during the measurement of the rate constant K. Through the compensation method, the error caused by using the data at different temperatures to calculate the activation energy can be reduced, leading to an improvement in accuracy for the optimization result. Using the ln A_α and E_α obtained under different conditions, the slope and intercept of the obtained line were a and b, respectively. Figure 7 shows the plot of the ln A_α versus E_α curves, which indicates the compensation effect [55]. Therefore, the linear relationship between pre-exponential factor and activation energy, where $a = 0.2006$, $b = -1.28471$ and $R^2 = 0.945$, is used to accurately predict pyrolysis kinetic parameters by eliminating various errors, thus enabling a more credible model to be established for the pyrolysis of chicken manure.

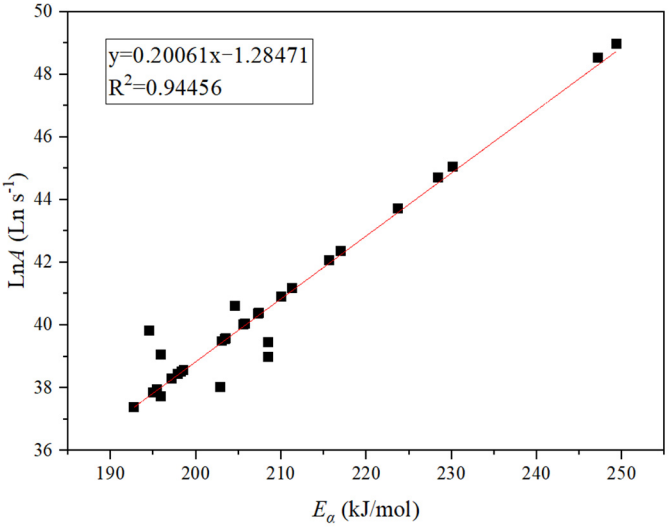

Figure 7. The compensation effect for chicken manure pyrolysis.

3.4. Thermodynamic Analysis

When determining the thermodynamic parameters of chicken manure, the lowest TGA heating rate (5 °C/min) is used. The low heating rate of TGA is known to be more accurate in reflecting thermal decomposition behavior and to derive thermodynamic values [56]. Owing to the lower heating rate, sufficient time is allowed for the heat transfer to occur, thereby enabling a complete pyrolysis behavior. The kinetics and thermodynamic parameter values calculated by the FWO, KAS and Friedman methods at different conversion fractions are shown in the Supplementary Material. For the Kissinger method, the use of the peak temperature from the heating rates allows a single global value to be derived, as shown in Table 5.

3.4.1. Pre-Exponential Value

The pre-exponential values (A) obtained by the FWO, KAS and Friedman methods are in the range of 10^{16} to 10^{21}, while those obtained by the Kissinger method are in the order of 10^{13}. In view of the complex components of chicken manure, this is also reflected in the pyrolysis behavior. When the conversion rate is 0.4, the increase in order of magnitude indicates the onset of cellulose and hemicellulose decomposition, which is also reflected in the need for more energy in the process. As the cellulose and hemicellulose are gradually decomposed, the energy requirement decreases and the values stabilize. At a conversion of 0.7, the value increases rapidly, mainly because the decomposition of the remaining lignin requires higher energy. The data in the table show the different energy levels required for different thermal degradation stages.

3.4.2. Enthalpy Change

ΔH represents the enthalpy change between the product and reactant. The positive value of enthalpy change for chicken manure pyrolysis is indicative of an endothermic reaction, in which the absorbed energy is used to break and form new chemical bonds. The activation energy mentioned earlier represents the energy required for the reaction to occur, so the difference between the enthalpy change of the reaction and the activation energy represents the difficulty of the reaction and can be used to evaluate the trend of the reaction. Taking the chicken manure pyrolysis data here as an example, the average difference between the enthalpy change of the reaction and the activation energy is less than 5 kJ/mol. This value belongs to a relatively low level, which indicates that the overall reaction is more favorable [57].

3.4.3. Gibbs Free Energy

Free energy refers to the part of the internal energy that the whole system reduces during the reaction process that can be converted into external work in the thermodynamic process. During biomass pyrolysis, the Gibbs free energy comes from the pyrolyzed biomass itself. The reduction of G in the reaction process is the maximum non-volume work done by the system and is the criterion for the direction and mode of the reaction. With the progress of chicken manure pyrolysis, the change of ΔG remained basically stable. The ΔG calculated in this study from three methods (FWO, KAS and Friedman) was between 153–156 kJ/mol, with a small variation range, indicating that the entire reaction had a relatively stable energy output.

3.4.4. Entropy Change

Entropy is a measure of the degree of disorder in a system. Change in entropy (ΔS) is related to changes in the number of reactants and products in the system before and after a reaction. It is a measure of how close the entire reaction system is to thermodynamic equilibrium. The results showed that ΔS value was low at the beginning of the reaction, accelerated and increased at the conversion rate of 0.4–0.5 as the reaction progressed, then leveled off, and finally reached a peak at the conversion rate of 0.7. Such a change trend shows that the pyrolysis of chicken manure is the most intense when the conversion rate is 0.4–0.5. This is because most of the components in chicken manure are in the process of decomposition when the conversion rate is 0.4–0.5. When the conversion rate reaches 0.7, the sudden increase in entropy is attributed to the reaction at higher temperature of other substances that have not been completely decomposed.

3.5. Estimation of Model Parameters by PSO Algorithm

Chicken manure is a typical lignocellulosic biomass, mainly composed of hemicellulose, cellulose and lignin, which has been tested by Rehman et al. [37]. The results are presented in Table 6.

Table 6. Composition of chicken manure [37].

Parameters	Chicken Manure
Water content (%)	77.18 ± 0.01
Dry mass (%)	22.82 ± 0.01
Cellulose (% dry mass)	14.49 ± 0.60
Hemicellulose (% dry mass)	21.66 ± 0.22
Lignin (% dry mass)	7.83 ± 0.12
TOC (% dry mass)	40.19 ± 0.90
TN (% dry mass)	3.54 ± 0.14
TP (% dry mass)	2.28 ± 0.08

TOC: total organic carbon; TN: total nitrogen; TP: total phosphorus.

For the decomposition of this type of biomass, a three-component reaction scheme is usually used. Equation (13) can be expressed as:

$$Hemicellulose \Rightarrow \lambda_1 Volatiles_1 + \delta_1 Char_1 \quad (24)$$

$$Cellulose \Rightarrow \lambda_2 Volatiles_2 + \delta_2 Char_2 \quad (25)$$

$$Lignin \Rightarrow \lambda_3 Volatiles_3 + \delta_3 Char_3 \quad (26)$$

The first, second and third subscripts represent the three pseudo-elements hemicellulose, cellulose and lignin, respectively.

3.5.1. Parameters Optimization

For the process of chicken manure pyrolysis, according to Equations (17) and (18), a total of 15 parameters needs to be optimized (E_i, A_i, n_i, δ_i and $W_{i,0}$, where i = 1, 2, 3).

Among them, E_i, A_i, and n_i are activation energy, pre-exponential factor and reaction order, respectively, which are the main parameters in kinetic analysis. $W_{i,0}$ represents the initial mass fraction of the raw material occupied by each component (the subscripts h, c, and l of W are the first letters of hemicellulose, cellulose and lignin, respectively), and δ_i is the coke yield during the reaction. Since $\sum W_{i,0} = 1$, the $W_{i,0}$ value of the lignin component can be calculated by $W_{i,0} = 1 - W_{h,0} - W_{c,0}$, which can reduce the number of unknowns in an optimization process, and improve the overall optimization speed and efficiency.

Vyazovkin et al. [58] proposed that kinetic parameters calculated from single-step reactions could be used as initial values in complex reaction optimization models. In the present work, the pyrolysis peak temperature T_P corresponding to each component under the five heating rates in the TG curve are used to calculate the kinetic parameters of E_α (activation energy) and A (pre-exponential factor) via the Kissinger method. The values calculated for the three components of hemicellulose, cellulose and lignin are used as the initial values $E_{0,i}$ and $A_{0,i}$ for each component in the optimization model. The lower and upper bounds of the search range for all the parameters to be optimized are set from 50 to 150% of the initial values. The initial values W of the mass fractions of the three components (i.e., hemicellulose, cellulose and lignin) are taken as $W_{h,0} = 0.20$, $W_{c,0} = 0.50$ and $W_{l,0} = 0.30$ [59]. The initial value for the reaction order n_i is assumed to be 1 and the search range is between 0–3 [60].

3.5.2. Kinetic Parameters Optimization

Table 7 lists the parameters and results of all optimized models. First, the optimized proportions of hemicellulose, cellulose and lignin are 23.8%, 44.2% and 32%, respectively, which are comparable to the range of composition values reported in the previous literature [61], i.e., 12–24% hemicelluloses, 43–54% cellulose, and 17–35% lignin. The optimized activation energy E_α values of, hemicellulose, cellulose and lignin are 118.98 kJ/mol, 227.8 kJ/mol and 134.26 kJ/mol, respectively. The obtained range of the pre-exponential factor ln A_α is between 15.75–26.98 ln/s, which is consistent with the range of 25.32–36.84 ln/s reported by de Jong et al. [62]. The optimized yield values for char (δ_i) and volatiles ($k_i = 1 - \delta_i$) for each reaction are also similar to the results of Front et al. [63]: the yield values for char for hemicellulose, cellulose and lignin are 17.7%, 38.7% and 20.1%, respectively. The data obtained from the optimization will be used to calculate the values for each point of the TG and DTG curves of the sample and its main components.

Table 7. Optimization parameters and results by particle swarm optimization (PSO).

Component	Parameters	Initial Values	Search Range	Optimized Values
Hemicellulose	*Ea*	118	(60, 180)	118.98
	ln*A*	26.07	(10, 40)	26.19
	δ(%)	23	(10, 35)	31.38
	n	1	(0, 3)	2.21
	W(%)	20	(10, 30)	23.8
Cellulose	*Ea*	167	(80, 250)	227.8
	ln*A*	27.67	(10, 45)	26.98
	δ(%)	6	(3, 9)	7.1
	n	1	(0, 3)	1.94
	W(%)	50	(25, 75)	44.2
Lignin	*Ea*	126	(60, 180)	134.26
	ln*A*	15.34	(5, 25)	15.75
	δ(%)	46	(20, 70)	37.2
	n	1	(0, 3)	0
	W(%)	30	(15, 45)	32

Figure 8 shows the calculated TG and DTG curves based on the optimized parameters compared with experimental data at 30 °C/min. The three pseudo-component (hemicellulose, cellulose and lignin) degradations are resolved and shown in the figure. The

decomposition behavior of each component is roughly similar to the overall pyrolysis process, albeit a lower decomposition rate of lignin can be clearly observed. By combining with the DTG curve, it can be seen that the decomposition of cellulose (~356 °C) requires a higher temperature than hemicellulose (~306 °C), while the pyrolysis peaks of hemicellulose and cellulose coincide with the adjacent two peaks of the overall pyrolysis process, thus validating the presence of cellulose substance. Furthermore, the decomposition of lignin is relatively slow throughout the entire pyrolysis process, but is seen to decompose at a faster rate at temperature around 410 °C. This also implies that lignin is more difficult to decompose than cellulose and hemicellulose.

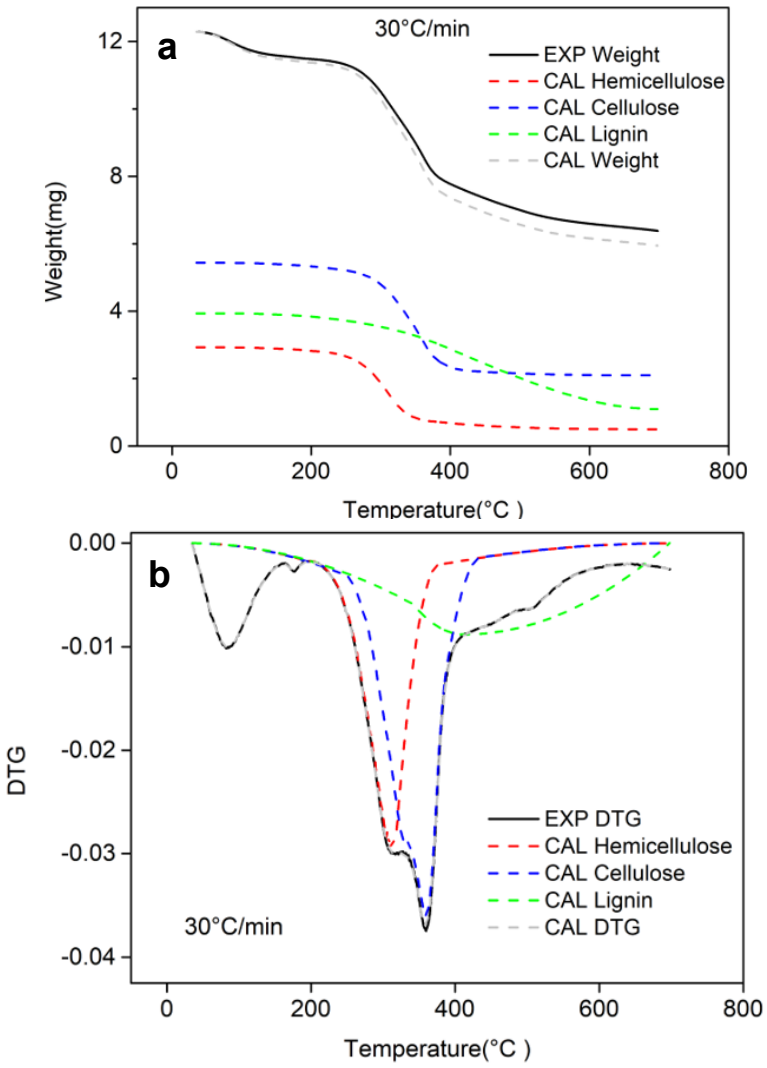

Figure 8. Calculated (**a**) TG and (**b**) DTG curves based on the optimized parameters compared with experimental data at 30 °C/min.

Figure 9 summarizes the experimental and predicted TG and DTG curves at five heating rates. It can be seen that the curve has a good fitting effect under each heating rate, while the fitting quality of the curve calculated based on Equation (22) is around 97%. This shows that the predicted TGA curves obtained by optimizing the experimental data are of high fidelity, thereby validating the use of the PSO algorithm to resolve and elucidate the chicken manure pyrolysis behavior.

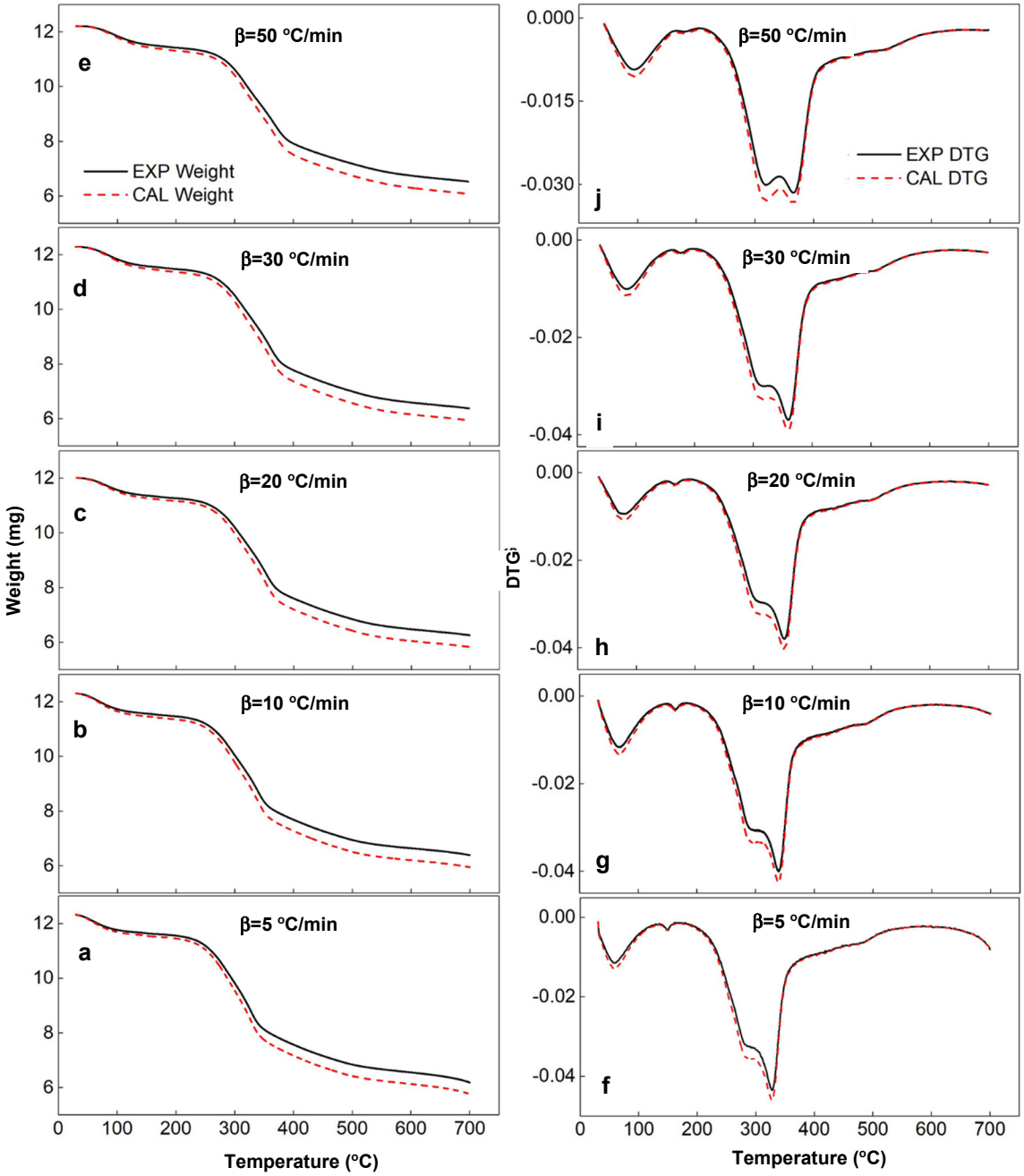

Figure 9. TG (left column: (**a**–**e**)) and DTG (right column: (**f**–**j**)) curves of different heating rates based on the calculated optimized parameters and experimental data.

4. Conclusions

In the present work, the pyrolysis characteristics of chicken manure were examined via thermogravimetric analysis at different heating rates. Subsequently, the kinetic parameters of chicken manure were determined via a non-isothermal pyrolysis process. The determined activation energies using iso-conversional model-free methods (FWO, KAS and Friedman) were 206.1, 200.6 and 231.9 kJ/mol, respectively, whereas the pre-exponential values were 1.68×10^{20}, 8.69×10^{19} and 1.65×10^{30} s^{-1}, respectively. The ability to capture the degradation behavior of different components at various conversion fractions leads to higher but more accurate values than those obtained using the Kissinger method (167.5 kJ/mol and 9.52×10^{13} s^{-1} for activation energy and pre-exponential factor, respectively), as the latter derives values from the overall reaction without accounting for the detailed kinetic mechanism.

To examine thermal degradation at the component level, the particle swarm optimization method was used to predict the kinetic parameters of each component via the three-component reaction scheme and the experimentally determined kinetic parameters as initial values. The optimized activation energy values obtained were 119.0 kJ/mol, 227.8 kJ/mol and 134.3 kJ/mol for hemicellulose, cellulose and lignin, respectively. Based on intrinsic transition-state theory, the pre-exponential factor and activation energy values fall within the range of Ln A_α = 0.2006 E_α − 1.2847, which results in optimized values and improved accuracy. The derived optimized parameters were then used to reproduce the pyrolysis curves as a function of temperature, which showed excellent matching with the experimental result of up to 97% in curve fitting quality. By combining the detailed kinetic analysis and advanced optimization algorithm, the pyrolysis behavior of chicken manure can be resolved down to component level. This work shows that kinetic data are useful as input parameters for optimization of the devolatilization process, as well as for the designing of thermochemical conversion processes for chicken manure.

Supplementary Materials: The following supporting information can be downloaded at: https://www.mdpi.com/article/10.3390/en16041919/s1, Table S1: Kinetics and thermodynamics parameters value calculated by FWO, KAS and Friedman methods at a heating rate of 5 °C/min.

Author Contributions: Conceptualization, C.T.C.; Methodology, J.G. and G.R.M.; Formal analysis, J.G.; Investigation, J.G.; Writing—original draft, J.G.; Writing—review & editing, C.T.C., G.R.M., J.-H.N. and W.W.F.C.; Supervision, C.T.C.; Funding acquisition, C.T.C. All authors have read and agreed to the published version of the manuscript.

Funding: The funding from Shanghai Jiao Tong University (BE2800001) is gratefully acknowledged.

Data Availability Statement: Data is available upon request.

Conflicts of Interest: The authors declare no conflict of interest.

References

1. UN Climate Change. What Is the Paris Agreement? 2021. Available online: https://unfccc.int/process-and-meetings/the-paris-agreement/the-paris-agreement (accessed on 30 November 2022).
2. UN Secretary-General. Carbon Neutrality by 2050: The World's Most Urgent Mission. 2020. Available online: https://www.un.org/sg/en/content/sg/articles/2020-12-11/carbon-neutrality-2050-the-world%E2%80%99s-most-urgent-mission (accessed on 1 December 2022).
3. Maxwell, A.-T.; Asiedu, N.; David, D.-A.; Karam, A.; Amaniampong, P.N. Thermochemical conversion and characterization of cocoa pod husks a potential agricultural waste from Ghana. *Ind. Crops Prod.* **2018**, *119*, 304–312.
4. Fodah, A.E.M.; Ghosal, M.K.; Behera, D. Microwave-assisted pyrolysis of agricultural residues: Current scenario, challenges, and future direction. *Int. J. Environ. Sci. Technol.* **2021**, *19*, 2195–2220. [CrossRef]
5. Li, K.; Zhang, L.; Zhu, L.; Zhu, X. Comparative study on pyrolysis of lignocellulosic and algal biomass using pyrolysis-gas chromatography/mass spectrometry. *Bioresour. Technol.* **2017**, *234*, 48–52. [CrossRef]
6. WATT Poultry. Poultry Dominates Meats in COVID World. Available online: https://www.wattagnet.com/articles/44017-poultry-dominates-meats-in-covid-world?v=preview (accessed on 29 November 2021).
7. FAO. Food and Agriculture Data. 2014. Available online: https://www.fao.org/faostat/zh/#home (accessed on 1 December 2022).
8. Bai, Z.; Li, X.; Lu, J.; Wang, X.; Velthof, G.L.; Chadwick, D.; Jiafa, L.; Ledgard, S.; Wu, Z.; Jin, S.; et al. Livestock housing and manure storage need to be improved in China. *Environ. Sci. Technol* **2017**, *51*, 8212–8214. [CrossRef]
9. Li, S.; Zou, D.; Li, L.; Wu, L.; Liu, F.; Zeng, X.; Wang, H.; Zhu, Y.; Xiao, Z. Evolution of heavy metals during thermal treatment of manure: A critical review and outlooks. *Chemosphere* **2020**, *247*, 125962. [CrossRef]
10. Qian, X.; Wang, Z.; Shen, G.; Chen, X.; Tang, Z.; Guo, C.; Gu, H.; Fu, K. Heavy metals accumulation in soil after 4 years of continuous land application of swine manure: A field-scale monitoring and modeling estimation. *Chemosphere* **2018**, *210*, 1029–1034. [CrossRef]
11. Rajat, N.; Agathe, A.; Bryan, K.M.; Paul, W.; Stephen, N.; Vincent, O.F.; Lauren, R.; Declan, B.; Owen, F.; Karl, R.; et al. Anaerobic digestion of agricultural manure and biomass—Critical indicators of risk and knowledge gaps. *Sci. Total Environ.* **2019**, *690*, 460–479.
12. Madhuri, G.; Prabhakar, P.; Anshuman, K.; Dharmesh, S.; Hemant, P. Study of microbial community plasticity for anaerobic digestion of vegetable waste in Anaerobic Baffled Reactor. *Renew. Energy* **2017**, *101*, 59–66.

13. Verma, M.; Godbout, S.; Brar, S.K.; Solomatnikova, O.; Lemay, S.P. Biofuels Production from Biomass by Thermochemical Conversion Technologies. *Int. J. Chem. Eng.* **2012**, *2012*, 542426. [CrossRef]
14. Mong, G.R.; Chong, C.T.; Ng, J.H.; Chong, W.W.F.; Lam, S.S.; Ong, H.C.; Ani, F.N. Microwave pyrolysis for valorisation of horse manure biowaste. *Energy Convers. Manag.* **2020**, *220*, 113074. [CrossRef]
15. Lee, J.; Choi, D.; Ok, Y.S.; Lee, S.-R.; Kwon, E.E. Enhancement of energy recovery from chicken manure by pyrolysis in carbon dioxide. *J. Clean. Prod.* **2017**, *164*, 146–152. [CrossRef]
16. Prabir, B. *Biomass Gasification, Pyrolysis and Torrefaction*, 3rd ed.; Elsevier: Amsterdam, The Netherlands, 2018.
17. Mei, B.; Ma, S.; Zhang, Y.; Zhang, X.; Li, W.; Li, Y. Exploration on laminar flame propagation of ammonia and syngas mixtures up to 10 atm. *Combust. Flame* **2020**, *220*, 368–377. [CrossRef]
18. Kathlene, J.A.; Kalpana, C.M.; Ajay, K.D. Bio-oil valorization: A review. *Renew. Sustain. Energy Rev.* **2013**, *23*, 91–106.
19. Ai, J.; Lu, C.; Frans, W.J.B.; Yin, W.; Bjarne, W.S.; Hans, C.B.H. Biochar catalyzed dechlorination—Which biochar properties matter? *J. Hazard. Mater.* **2021**, *406*, 124724. [CrossRef]
20. Zhang, Y.; Cui, Y.; Liu, S. Fast microwave-assisted pyrolysis of wastes for biofuels production—A review. *Bioresour. Technol.* **2020**, *297*, 122480. [CrossRef]
21. Wang, T.; Liu, H.; Duan, C.; Xu, R.; Zhang, Z. The Eco-Friendly Biochar and Valuable Bio-Oil from Caragana korshinskii: Pyrolysis Preparation, Characterization, and Adsorption Applications. *Materials* **2020**, *13*, 3391. [CrossRef]
22. Xu, T.; Xu, F.; Hu, Z.; Chen, Z.; Xiao, B. Non-isothermal kinetics of biomass-pyrolysis-derived-tar (BPDT) thermal decomposition via thermogravimetric analysis. *Energy Convers. Manag.* **2017**, *138*, 452–460. [CrossRef]
23. Dhyani, V.; Kumar, A.M.; Wang, Q.; Kumar, J.; Ren, X.; Zhao, J.; Chen, H.; Wang, M.; Bhaskar, T.; Zhang, Z. Effect of composting on the thermal decomposition behavior and kinetic parameters of pig manure-derived solid waste. *Bioresour. Technol.* **2018**, *252*, 59–65. [CrossRef]
24. Huang, X.; Cao, J.; Zhao, X.; Wang, J.; Fan, X.; Zhao, Y.; Wei, X. Pyrolysis kinetics of soybean straw using thermogravimetric analysis. *Fuel* **2016**, *169*, 93–98. [CrossRef]
25. Mishra, R.K.; Mohanty, K. Pyrolysis kinetics and thermal behavior of waste sawdust biomass using thermogravimetric analysis. *Bioresour. Technol.* **2018**, *251*, 63–74. [CrossRef]
26. Slopiecka, K.; Bartocci, P.; Fantozzi, F. Thermogravimetric analysis and kinetic study of poplar wood pyrolysis. *Appl. Energy* **2012**, *97*, 491–497. [CrossRef]
27. Cao, H.; Xin, Y.; Wang, D.; Yuan, Q. Pyrolysis characteristics of cattle manures using a discrete distributed activation energy model. *Bioresour. Technol.* **2014**, *172*, 219–225. [CrossRef]
28. Chong, C.T.; Mong, G.R.; Ng, J.H.; Chong, W.W.F.; Ani, F.N.; Lam, S.S.; Ong, H.C. Pyrolysis characteristics and kinetic studies of horse manure using thermogravimetric analysis. *Energy Convers. Manag.* **2019**, *180*, 1260–1267. [CrossRef]
29. Fernandez-Lopez, M.; Pedrosa-Castro, G.J.; Valverde, J.L.; Sanchez-Silva, L. Kinetic analysis of manure pyrolysis and combustion processes. *Waste Manag.* **2016**, *58*, 230–240. [CrossRef]
30. Ding, Y.; Zhang, J.; He, Q.; Huang, B.; Mao, S. The application and validity of various reaction kinetic models on woody biomass pyrolysis. *Energy* **2019**, *179*, 784–791. [CrossRef]
31. He, S.; Cao, C.; Wang, J.; Yang, J.; Cheng, Z.; Pan, Y.; Chen, G. Pyrolysis study on cattle manure: From conventional analytical method to online study of pyrolysis photoionization time-of-flight mass spectrometry. *J. Anal. Appl. Pyrolysis* **2020**, *151*, 104916. [CrossRef]
32. Li, K.-Y.; Huang, X.; Fleischmann, C.; Ji, J. Pyrolysis of Medium-Density Fiberboard: Optimized Search for Kinetics Scheme and Parameters via a Genetic Algorithm Driven by Kissinger's Method. *Energy Fuels* **2014**, *28*, 6130–6139. [CrossRef]
33. Bianchi, O.; Oliveira, R.V.B.; Fiorio, R.; Martins, J.D.N.; Zattera, A.J.; Canto, L.B. Assessment of Avrami, Ozawa and Avrami–Ozawa equations for determination of EVA crosslinking kinetics from DSC measurements. *Polym. Test.* **2008**, *27*, 722–729. [CrossRef]
34. Clemente-Castro, S.; Palma, A.; Ruiz-Montoya, M.; Giráldez, I.; Díaz, M.J. Pyrolysis kinetic, thermodynamic and product analysis of different leguminous biomasses by Kissinger-Akahira-Sunose and pyrolysis-gas chromatography-mass spectrometry. *J. Anal. Appl. Pyrolysis* **2022**, *162*, 105457. [CrossRef]
35. Venkatesh, M.; Ravi, P.; Tewari, S.P. Isoconversional Kinetic Analysis of Decomposition of Nitroimidazoles: Friedman method vs. Flynn–Wall–Ozawa Method. *J. Phys. Chem. A Mol. Spectrosc. Kinet. Environ. Gen. Theory* **2013**, *117*, 10162–10169. [CrossRef]
36. Vyazovkin, S. Kissinger Method in Kinetics of Materials: Things to Beware and Be Aware of. *Molecules* **2020**, *25*, 2813. [CrossRef]
37. Kashif, R.; Cai, M.; Xiao, X.; Zheng, L.; Wang, H.; Abdul, A.S.; Zhou, Y.; Li, W.; Yu, Z.; Zhang, J. Cellulose decomposition and larval biomass production from the co-digestion of dairy manure and chicken manure by mini-livestock (*Hermetia illucens* L.). *J. Environ. Manag.* **2017**, *196*, 458–465.
38. Mohammed, E.A. Performance assessment of foraging algorithms vs. evolutionary algorithms. *Inf. Sci.* **2012**, *182*, 243–263.
39. Li, X.; Lu, Q.; Dong, Y.; Tao, D. SCE: A Manifold Regularized Set-Covering Method for Data Partitioning. *IEEE Trans. Neural Netw. Learn. Syst.* **2018**, *29*, 1760–1773. [CrossRef]
40. Majid, M.; Chin, B.L.F.; Jawad, Z.A.; Chai, Y.; Lam, M.K.; Yusup, S.; Cheah, K.W. Particle swarm optimization and global sensitivity analysis for catalytic co-pyrolysis of Chlorella vulgaris and plastic waste mixtures. *Bioresour. Technol.* **2021**, *329*, 124874. [CrossRef]
41. Bui, H.; Tran, K.; Chen, W. Pyrolysis of microalgae residues—A kinetic study. *Bioresour. Technol.* **2016**, *199*, 362–366. [CrossRef]

42. Kim, Y.S.; Kim, Y.S.; Kim, S.H. Investigation of Thermodynamic Parameters in the Thermal Decomposition of Plastic Waste-Waste Lube Oil Compounds. *Environ. Sci. Technol.* **2010**, *44*, 5313–5317. [CrossRef] [PubMed]
43. Chen, W.; Lin, B.; Huang, M.; Chang, J. Thermochemical conversion of microalgal biomass into biofuels: A review. *Bioresour. Technol.* **2015**, *184*, 314–327. [CrossRef]
44. Luqman, R.; Wang, Q.; Yang, Q.; Lia, X.; Yuan, W. Potential of industrial composting and anaerobic digestion for the removal of antibiotics, antibiotic resistance genes and heavy metals from chicken manure. *Sci. Total Environ.* **2020**, *718*, 137414.
45. Das, K.C.; Garcia-perez, M.; Bibens, B.; Melear, N.P.; Taylor & Francis Group. Slow pyrolysis of poultry litter and pine woody biomass: Impact of chars and bio-oils on microbial growth. *J. Environ. Sci. Health* **2008**, *43*, 714–724. [CrossRef] [PubMed]
46. Osama, M.S.; Ryoichi, S.A. Co-Pyrolysis of Chicken and Cow Manure. *J. Energy Resour. Technol* **2021**, *143*, 011301.
47. Juan, E.; Osama, M.S.; Ryoichi, S.A. Co-Pyrolysis of Rice Husk and Chicken Manure. *J. Energy Resour. Technol* **2021**, *142*, 022101.
48. Barneto, A.G.; Carmona, J.A.; Alfonso, J.E.M.; Serrano, R.S. Simulation of the thermogravimetry analysis of three non-wood pulps. *Bioresour. Technol.* **2010**, *101*, 3220–3229. [CrossRef]
49. Cai, J.; Xu, D.; Dong, Z.; Yu, X.; Yang, Y.; Banks, S.W.; Bridgwater, A.V. Processing thermogravimetric analysis data for isoconversional kinetic analysis of lignocellulosic biomass pyrolysis: Case study of corn stalk. *Renew. Sustain. Energy Rev.* **2018**, *82*, 2705–2715. [CrossRef]
50. Buyukada, M. Data-driven nonlinear modeling studies on removal of Acid Yellow 59 using Si-doped multi-walled carbon nanotubes. *Int. J. Environ. Sci. Technol.* **2017**, *14*, 2215–2228. [CrossRef]
51. Vyazovkin, S.; Wight, C.A. Model-free and model-fitting approaches to kinetic analysis of isothermal and nonisothermal data. *Thermochim. Acta* **1999**, *340*, 53–68. [CrossRef]
52. Popescu, C. Integral method to analyze the kinetics of heterogeneous reactions under non-isothermal conditions A variant on the Ozawa-Flynn-Wall method. *Thermochim. Acta* **1996**, *285*, 309–323. [CrossRef]
53. Ammar, K.; Douglas, R.F. Solid-State Kinetic Models: Basics and Mathematical Fundamentals. *J. Phys. Chem. B* **2006**, *110*, 17315–17328.
54. Xu, L.; Jiang, Y.; Wang, L. Thermal decomposition of rape straw: Pyrolysis modeling and kinetic study via particle swarm optimization. *Energy Convers. Manag.* **2017**, *146*, 124–133. [CrossRef]
55. Patrick, J.B. The mathematical origins of the kinetic compensation effect: 2. the effect of systematic errors. *Phys. Chem. Chem. Phys.* **2012**, *14*, 327–336.
56. He, Y.; Chang, C.; Li, P.; Han, X.; Li, H.; Fang, S.; Chen, J.; Ma, X. Thermal decomposition and kinetics of coal and fermented cornstalk using thermogravimetric analysis. *Bioresour. Technol.* **2018**, *259*, 294–303. [CrossRef] [PubMed]
57. Ahmad Muhammad, S.; Mehmood Muhammad, A.; Taqvi, S.T.H.; Elkamel, A.; Liu, C.G.; Xu, J.R.; Rahimuddin, S.A.; Gull, M. Pyrolysis, kinetics analysis, thermodynamics parameters and reaction mechanism of Typha latifolia to evaluate its bioenergy potential. *Bioresour. Technol.* **2017**, *245*, 491–501. [CrossRef]
58. Vyazovkin, S.; Burnham, A.K.; Criado, J.M.; Pérez-Maqueda, L.A.; Popescu, C.; Sbirrazzuoli, N. ICTAC Kinetics Committee recommendations for performing kinetic computations on thermal analysis data. *Thermochim. Acta* **2011**, *520*, 1–19. [CrossRef]
59. Yang, H.; Chen, H.; Zheng, C.; Yan, R.; Lee, D.H. Characteristics of hemicellulose, cellulose and lignin pyrolysis. *Fuel* **2007**, *86*, 1781–1788. [CrossRef]
60. Becidan, M.; Hustad, J.E.; Skreiberg, Ø.; Várhegyi, G. Thermal decomposition of biomass wastes. A kinetic study. *Ind. Eng. Chem. Res.* **2007**, *46*, 2428–2437. [CrossRef]
61. Munir, S.; Daood, S.S.; Nimmo, W.; Cunliffe, A.M.; Gibbs, B.M. Thermal analysis and devolatilization kinetics of cotton stalk, sugar cane bagasse and shea meal under nitrogen and air atmospheres. *Bioresour. Technol.* **2009**, *100*, 1413–1418. [CrossRef]
62. De Jong, W.; Di Nola, G.; Venneker BC, H.; Spliethoff, H.; Wojtowicz, M.A. TG-FTIR pyrolysis of coal and secondary biomass fuels: Determination of pyrolysis kinetic parameters for main species and NOx precursors. *Fuel* **2007**, *86*, 2367–2376. [CrossRef]
63. Font, R.; Conesa, J.A.; Moltó, J.; Muñoz, M. Kinetics of pyrolysis and combustion of pine needles and cones. *J. Anal. Appl. Pyrolysis* **2009**, *85*, 276–286. [CrossRef]